

# Non-linear evolution of $f(R)$ cosmologies II: power spectrum

Hiroaki Oyaizu,<sup>1,2</sup> Marcos Lima,<sup>1,3</sup> and Wayne Hu<sup>1,2</sup>

<sup>1</sup>*Kavli Institute for Cosmological Physics, and Enrico Fermi Institute, University of Chicago, Chicago IL 60637*

<sup>2</sup>*Department of Astronomy & Astrophysics, University of Chicago, Chicago IL 60637*

<sup>3</sup>*Department of Physics, University of Chicago, Chicago IL 60637*

(Dated: November 1, 2018)

We carry out a suite of cosmological simulations of modified action  $f(R)$  models where cosmic acceleration arises from an alteration of gravity instead of dark energy. These models introduce an extra scalar degree of freedom which enhances the force of gravity below the inverse mass or Compton scale of the scalar. The simulations exhibit the so-called chameleon mechanism, necessary for satisfying local constraints on gravity, where this scale depends on environment, in particular the depth of the local gravitational potential. We find that the chameleon mechanism can substantially suppress the enhancement of power spectrum in the non-linear regime if the background field value is comparable to or smaller than the depth of the gravitational potentials of typical structures. Nonetheless power spectrum enhancements at intermediate scales remain at a measurable level for models even when the expansion history is indistinguishable from a cosmological constant, cold dark matter model. Simple scaling relations that take the linear power spectrum into a non-linear spectrum fail to capture the modifications of  $f(R)$  due to the change in collapsed structures, the chameleon mechanism, and the time evolution of the modifications.

## I. INTRODUCTION

Cosmic acceleration can arise from either an exotic form of energy with negative pressure or a modification to gravity in the infrared. Self-consistent models for the latter are highly constrained by the stringent tests of gravity in the solar system. Additional propagating degrees of freedom must be suppressed by non-linearities in their equations of motion [1, 2, 3] in a stable manner [4, 5, 6]. These suppression mechanisms manifest themselves with the formation of non-linear structure in the Universe [7, 8, 9]. Understanding the physical content, phenomenology and even the basic viability of such models thus requires cosmological simulations.

One possibility that has received much recent attention is the so-called  $f(R)$  class of models (see [10] and references therein). These models generate acceleration through a replacement of the Einstein-Hilbert action by a function of the Ricci or curvature scalar  $R$  [11, 12, 13]. They also introduce an extra propagating scalar degree of freedom that acts as an effective fifth force on all forms of matter [14, 15]. The range of the force depends non-linearly on the local curvature and can be made to become infinitesimal at high curvature. With an appropriate choice of the function  $f(R)$ , deep potential regions can trap the field at high curvature leading to a non-linear “chameleon mechanism” [16] that suppresses local deviations from ordinary gravity [17, 18, 19].

Whether or not solar system tests of gravity are satisfied in an  $f(R)$  model then depends on the depth of the gravitational potential including the astrophysical and cosmological structure surrounding it [19]. Likewise observable deviations from ordinary gravity for upcoming dark energy probes such as weak lensing, galaxy clustering and clusters of galaxies depend on the whole history of non-linear structure formation.

Previous cosmological simulations (*e.g.* [20, 21, 22, 23,

24]) have focused on modifications of the force law with a fixed and density independent range. Such modifications alone are incapable of satisfying local tests of gravity.

In a companion paper [25], the numerical methodology for solving the non-linear field equation of  $f(R)$  gravity was established. In this second paper of the series, we apply this methodology and carry out a suite of cosmological simulations of  $f(R)$  models that are chosen to expose the impact of the chameleon mechanism on the power spectrum of the matter and the lensing potential.

We begin in §II with a review of non-linear gravitational dynamics in  $f(R)$  models and proceed to the simulation results in §III. We discuss these results in §IV.

## II. $f(R)$ DYNAMICS

### A. Basic equations

The class of modifications we consider generalizes the Einstein-Hilbert action to include an arbitrary function  $f(R)$  of the scalar curvature  $R$

$$S = \int d^4x \sqrt{-g} \left[ \frac{R + f(R)}{16\pi G} + L_m \right]. \quad (1)$$

Here  $L_m$  is the Lagrangian of the ordinary matter which remains minimally coupled. Setting  $f(R) = 0$  recovers general relativity (GR) without a cosmological constant whereas setting  $f(R) = -16\pi G\rho_\Lambda = \text{const.}$  recovers it with a cosmological constant. Here and throughout  $c = \hbar = 1$ .

Variation of Eq. (1) with respect to the metric yields the modified Einstein equations

$$\begin{aligned} G_{\alpha\beta} + F_{\alpha\beta} &= 8\pi G T_{\alpha\beta}, \\ F_{\alpha\beta} &= f_R R_{\alpha\beta} - \left( \frac{f}{2} - \square f_R \right) g_{\alpha\beta} - \nabla_\alpha \nabla_\beta f_R, \end{aligned} \quad (2)$$

where the field,

$$f_R \equiv \frac{df(R)}{dR}, \quad (3)$$

plays the role of a propagating extra scalar degree of freedom. In particular the trace of the modified Einstein equation (2) yields the equation of motion for the field

$$\square f_R = \frac{\partial V_{\text{eff}}}{\partial f_R}, \quad (4)$$

with the effective potential defined by

$$\frac{\partial V_{\text{eff}}}{\partial f_R} \equiv \frac{1}{3} [R - f_R R + 2f - 8\pi G(\rho - 3p)]. \quad (5)$$

The effective potential has an extremum at

$$R - Rf_R + 2f = 8\pi G(\rho - 3p), \quad (6)$$

and its curvature is given by

$$\mu^2 = \frac{\partial^2 V_{\text{eff}}}{\partial f_R^2} = \frac{1}{3} \left( \frac{1 + f_R}{df_R/dR} - R \right). \quad (7)$$

This can be interpreted as the effective mass of the field  $f_R$  and defines the range of the force. For stability, the extremum should be a minimum and hence  $\mu^2 > 0$  [5].

Phenomenologically viable models typically must have very flat  $f(R)$  functions such that  $|f_R| \ll 1$  at cosmological curvatures and larger. The model we simulate is in the class of  $f(R)$  functions proposed in [19],

$$f(R) \propto \frac{R}{AR + 1}, \quad (8)$$

where  $A$  is a constant with dimensions of length squared. In the limit  $R \rightarrow 0$ ,  $f(R) \rightarrow 0$  as with GR with no cosmological constant. For sufficiently high curvature that  $AR \gg 1$ ,  $f(R)$  can be approximated as a constant, which drives the acceleration, plus a term that is inversely proportional to curvature. In this limit, we can approximate Eq. (8) by

$$f(R) \approx -16\pi G\rho_\Lambda - f_{R0} \frac{\bar{R}_0^2}{R}, \quad (9)$$

where we have set the constant  $A$  to match some effective cosmological constant  $\rho_\Lambda$ . Here we define  $\bar{R}_0 = \bar{R}(z=0)$  as the background curvature today and  $f_{R0} = f_R(\bar{R}_0)$ .

Taking  $|f_{R0}| \ll 1$ , the background expansion follows the  $\Lambda$ CDM history with the same  $\rho_\Lambda$  to leading order in  $|f_{R0}|$  [19]. In particular the background curvature may be approximated as

$$\bar{R} \approx 3H_0^2 [\Omega_m(1+z)^3 + 4\Omega_\Lambda], \quad (10)$$

where  $\Omega_i = 8\pi G\rho_i(z=0)/3H_0^2$ . We can also simplify the mass term in Eq. (7)  $\mu \approx (3df_R/dR)^{-1/2}$  defining

the comoving Compton wavelength or range of the field  $\lambda_C$  as

$$\frac{\lambda_C}{1+z} = \mu^{-1} \approx \sqrt{6|f_{R0}|} \frac{R_0^2}{R^3}. \quad (11)$$

Notice that the range of the interaction has a steep inverse dependence on the local curvature  $R$ .

We take the WMAP3 [26] flat background cosmology throughout:  $\Omega_m = 0.24$ ,  $\Omega_\Lambda = 0.76$ ,  $\Omega_b = 0.04181$ ,  $H_0 = 73$  km/s/Mpc, and initial power in curvature fluctuations  $A_s = (4.52 \times 10^{-5})^2$  at  $k = 0.05 \text{ Mpc}^{-1}$  with a tilt of  $n_s = 0.958$ . For  $\Lambda$ CDM these parameters give  $\sigma_8 = 0.76$ .

For these values, the Compton wavelength for the background today is

$$\lambda_{C0} \approx 3.2 \sqrt{\frac{|f_{R0}|}{10^{-6}}} \text{ Mpc}. \quad (12)$$

Note that even for field amplitudes as low as  $|f_{R0}| \approx 10^{-7}$  where deviations from  $\Lambda$ CDM in the expansion history are comparably negligible, the modifications to gravity at the cosmological background density are order unity at astrophysically interesting scales of a Mpc [19].

Furthermore, the field equation (4) can be simplified by neglecting the small  $f_R R$  term and assuming that matter dominates over radiation, thus resulting in

$$\square f_R = \frac{1}{3} [R - 8\pi G(\rho_m + 4\rho_\Lambda)]. \quad (13)$$

Subtracting off the background values for the field, curvature and density yields

$$\square \delta f_R = \frac{1}{3} [\delta R(f_R) - 8\pi G\delta\rho_m], \quad (14)$$

where  $\delta R \equiv R - \bar{R}$ ,  $\delta f_R = f_R - f_R(\bar{R})$ ,  $\delta\rho_m = \rho_m - \bar{\rho}_m$ . Note that the field fluctuation is defined by subtracting off the field evaluated at the background curvature and not the spatially averaged field value. The procedure eliminates the potential ambiguity of defining fluctuations with a highly non-linear field equation.

The minimum of the effective potential is at a curvature corresponding to the GR expectation  $\delta R = 8\pi G\delta\rho_m$ . If the field value achieves this minimum then the high density regions have high curvature and short Compton wavelengths which suppress the deviations from ordinary gravity. However, we shall see in §II B that whether the field value achieves this minimum at any given location depends on the depth of the gravitational potential.

Finally, we work on scales much less than the horizon such that the quasi-static limit applies where time derivatives may be neglected compared with spatial derivatives. This corresponds to assuming that the field instantaneously relaxes to its equilibrium value. More specifically, relaxation must occur on a time scale that is short compared with the non-relativistic motion of particles. This approximation should be excellent for wavelengths that are not orders of magnitude larger than the Compton scale below which field perturbations propagate near

the speed of light. The field equation in comoving coordinates then becomes a non-linear Poisson-type equation

$$\nabla^2 \delta f_R = \frac{a^2}{3} [\delta R(f_R) - 8\pi G \delta \rho_m]. \quad (15)$$

An explicit consistency test of this approximation in the cosmological context is given in [25].

Since  $f(R)$  is a metric theory of gravity, particles move in the metric or gravitational potential in the same way as in general relativity. However the field acts as a source that distinguishes the two potentials in the metric

$$ds^2 = -(1 + 2\Psi)dt^2 + a^2(1 + 2\Phi)dx^2. \quad (16)$$

In the quasi-static limit, the modified Einstein equations (2) imply that the Newtonian potential  $\Psi$ , whose gradient is responsible for the motion of particles, is given by a Poisson equation that is linear in  $\delta \rho_m$  and  $\delta R$  [27],

$$\nabla^2 \Psi = \frac{16\pi G}{3} a^2 \delta \rho_m - \frac{a^2}{6} \delta R(f_R). \quad (17)$$

Equations (15) and (17) define a closed system for the gravitational potential given the density field. It is interesting to note that braneworld modified gravity models [28] obey a similar system of equations except that the effective potential involves field gradients [8].

## B. Non-linear chameleon

Before proceeding to the numerical solution of these equations, it is worthwhile to examine the qualitative aspects of the  $f(R)$  system of equations to expose potential observational consequences. In particular, these equations exhibit the chameleon mechanism under which modifications to gravity become environment dependent.

The force law modifications are manifested by the appearance of the second potential  $\Phi$  in Eq. (16). Gravitational lensing and redshifts of photons depend on a combination of the two potentials

$$\nabla^2 \frac{(\Phi - \Psi)}{2} = -4\pi G a^2 \delta \rho_m, \quad (18)$$

Note that this relationship between the lensing potential and the matter density is unaltered from the GR expectation. It is the Poisson equation for  $\Psi$  that has an altered relationship to the matter density and governs the motion of non-relativistic particles. Ordinary gravity is recovered if  $\delta R = 8\pi G \delta \rho_m$ , and the equation for the gravitational potential reduces to the unmodified equation,

$$\nabla^2 \Psi = 4\pi G a^2 \delta \rho_m, \quad (19)$$

and

$$\frac{(\Phi - \Psi)}{2} = \Phi = -\Psi. \quad (20)$$

Deviation from this relation locally are constrained by solar system tests of gravity at the level of  $|(\Phi + \Psi)/\Psi| \lesssim 10^{-5}$  [29]. These deviations are related to changes in the field through the field equation (15), the Poisson equation (17) and the lensing potential (18)

$$\nabla^2(\Phi + \Psi) = -\nabla^2 \delta f_R. \quad (21)$$

If the force modifications are small, then  $|(\Phi + \Psi)/\Psi| \ll 1$  for local contributions to the potential.

This relationship gives a rule of thumb for the appearance of the chameleon effect. Consider an isolated spherically symmetric structure embedded in the background density. At the center of the object, the change in the field is related to the total depth of the potentials as

$$\Delta f_R = -(\Phi + \Psi), \quad (22)$$

as long as both remain finite at the center.

To drive the range of the force modification to a scale much smaller than the background value, the field amplitude  $|f_R|$  must be substantially below its background value  $|f_{\bar{R}}|$  at the center. For example, at the current epoch this requires

$$|\Delta f_R| \sim |f_{R0}| \sim |\Phi + \Psi| \ll |\Psi|. \quad (23)$$

This is a necessary condition for the appearance of a chameleon. A chameleon also does not appear if most of the mass contributing to  $\Psi$  is on scales above the Compton scale of the background. In this case  $|\Phi + \Psi|$  remains much smaller than  $\Psi$  in this regime and the change in potential does not contribute to a substantial change in the field  $\Delta f_R$ . Thus the smooth potential contributed by very large scale structure does not enter into the chameleon suppression.

If the local potential is not sufficiently deep, the field prefers to remain smooth at the background value and not track  $\delta R(f_R) = 8\pi G \delta \rho_m$ . Energetically, the cost of high field gradients prevents the field from lying at the local minimum of the effective potential [19]. In this case the field remains near its background value and  $\delta R(f_R) \ll 8\pi G \delta \rho_m$ . Eq. (17) then implies that the strength of gravity is a factor of 4/3 greater than ordinary gravity.

This consequence can alternatively be seen directly through Eq. (15). If the field fluctuation is small then  $\delta R \approx (dR/df_R)\delta f_R$  and the field equation can be solved in Fourier space as a linear Poisson equation

$$\delta f_R(\mathbf{k}) = \frac{1}{3} \frac{8\pi G a^2 \delta \rho_m(\mathbf{k})}{k^2 + a^2 \bar{\mu}^2}, \quad (24)$$

where  $\bar{\mu} = \mu(\bar{R})$  and defines the Compton scale in the background through Eq. (11). This solution combined with the Poisson equation (17) gives

$$k^2 \Psi(\mathbf{k}) = -4\pi G \left( \frac{4}{3} - \frac{1}{3} \frac{\mu^2 a^2}{k^2 + \bar{\mu}^2 a^2} \right) a^2 \delta \rho_m(\mathbf{k}), \quad (25)$$

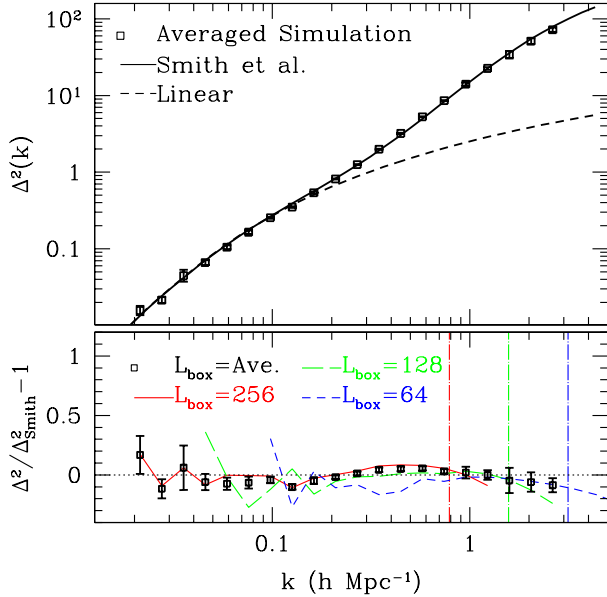


FIG. 1: The mean power spectra  $\Delta^2 = k^3 P(k)/2\pi^2$  of the cosmological simulations without  $f_R$  modifications ( $\Lambda$ CDM or  $|f_{R0}| = 0$ ). *Upper panel:* Average power spectrum of all simulations in comparison to linear theory and the Smith *et al.* non-linear fit (solid line). *Lower panel:* Relative power spectrum offset from Smith *et al.* fit. The individual simulation box sizes averages are plotted in solid, long-dashed, and dashed lines. Results converge at approximately the half-Nyquist wavenumbers (vertical lines). Points with errors show the mean and the  $1\text{-}\sigma$  error bars computed using the bootstrap method, weighted by simulation box volume, out to the half-Nyquist wavenumbers (see text).

which has an effective  $G$  that depends on wavelength such that  $G \rightarrow 4/3G$  below the Compton wavelength in the background. Note that linearity in the density field is *not* assumed. Hence we will use this field linearization approximation to test the effects of the chameleon in the simulations.

In summary order unity modifications to gravity are expected on scales smaller than the Compton scale of the background but away from the centers of deep gravitational potential wells of cosmological structure. In these regions, the chameleon mechanism suppresses the local Compton scale and hence the force modifications.

### III. $f(R)$ SIMULATIONS

#### A. Simulation description

To solve the system of equations defined by the modified Poisson equation (17) and the quasi-static  $f_R$  field equation (15) in the context of cosmological structure formation, we employ the methodology described in [25]. Briefly, the field equation for  $f_R$  is solved on a regular grid using relaxation techniques and multigrid iteration [30, 31]. The potential  $\Psi$  is computed from the density

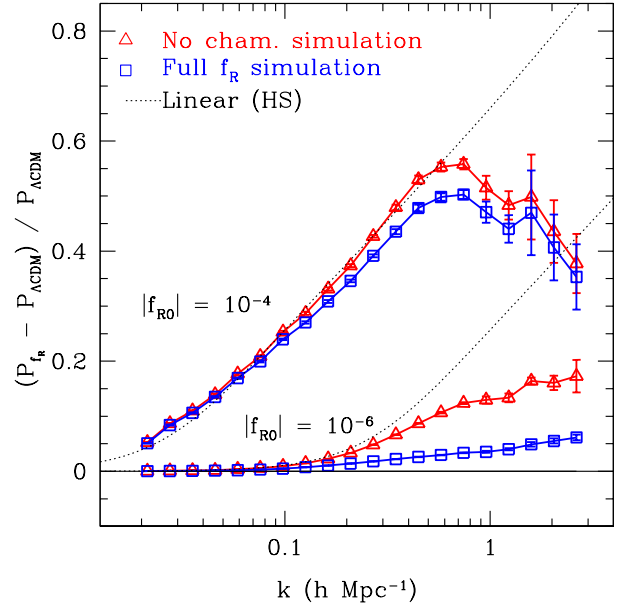


FIG. 2: Relative power spectrum enhancement over  $\Lambda$ CDM at  $a = 1$  for the full  $f_R$  simulation compared with the no-chameleon  $f_R$  simulations and linear theory. At high  $k$ , linear theory underestimates the absolute power for both  $\Lambda$ CDM and  $f_R$  while overestimating the relative enhancement. Without the chameleon, power is sharply enhanced on scales smaller than the Compton scale in the background which increases with  $|f_{R0}|$  (see Eq. (12)). For  $|f_{R0}| = 10^{-6}$  the chameleon strongly suppresses these enhancements at high  $k$ . For  $|f_{R0}| = 10^{-4}$ , this suppression is nearly absent except for a residual effect from the chameleon at high redshift. The 3 highest points in  $k$  have increased sampling errors since they utilize only the  $64h^{-1}$  Mpc boxes. Note that the linear prediction is the fractional enhancement in the *linear* power spectrum, that is,  $(P_{f_R, \text{linear}} - P_{\Lambda\text{CDM}, \text{linear}})/P_{\Lambda\text{CDM}, \text{linear}}$ .

and  $f_R$  fields using the fast Fourier transform method. The dark matter particles are then moved according to the gradient of the computed potential,  $-\nabla\Psi$ , using a second order accurate leap-frog integrator.

Since the Compton wavelength or range of the  $f_R$  field in Eq. (11) shrinks with increasing curvature, modifications to the force law and structure formation above any given comoving scale vanish at sufficiently high redshift. We can therefore treat the initial conditions for the simulations in the same way as in a cosmology with ordinary gravity. All simulations have the cosmological parameters given in the previous section which make them all compatible with the high redshift CMB observations from WMAP [32]. To explore the modifications induced by the  $f_R$  field, we simulate models with field strengths in the background of  $|f_{R0}| = 0, 10^{-6}, 10^{-5}, 10^{-4}$ . Note that the  $|f_{R0}| = 0$  is exactly equivalent to  $\Lambda$ CDM.

Specifically, the initial conditions for the simulations are created using Enzo [33], a publicly available cosmological N-body + hydrodynamics code. Enzo uses the Zel'dovich approximation to displace particles on a uniform grid according to a given initial power spectrum. We use the initial power spectra given by the transfer



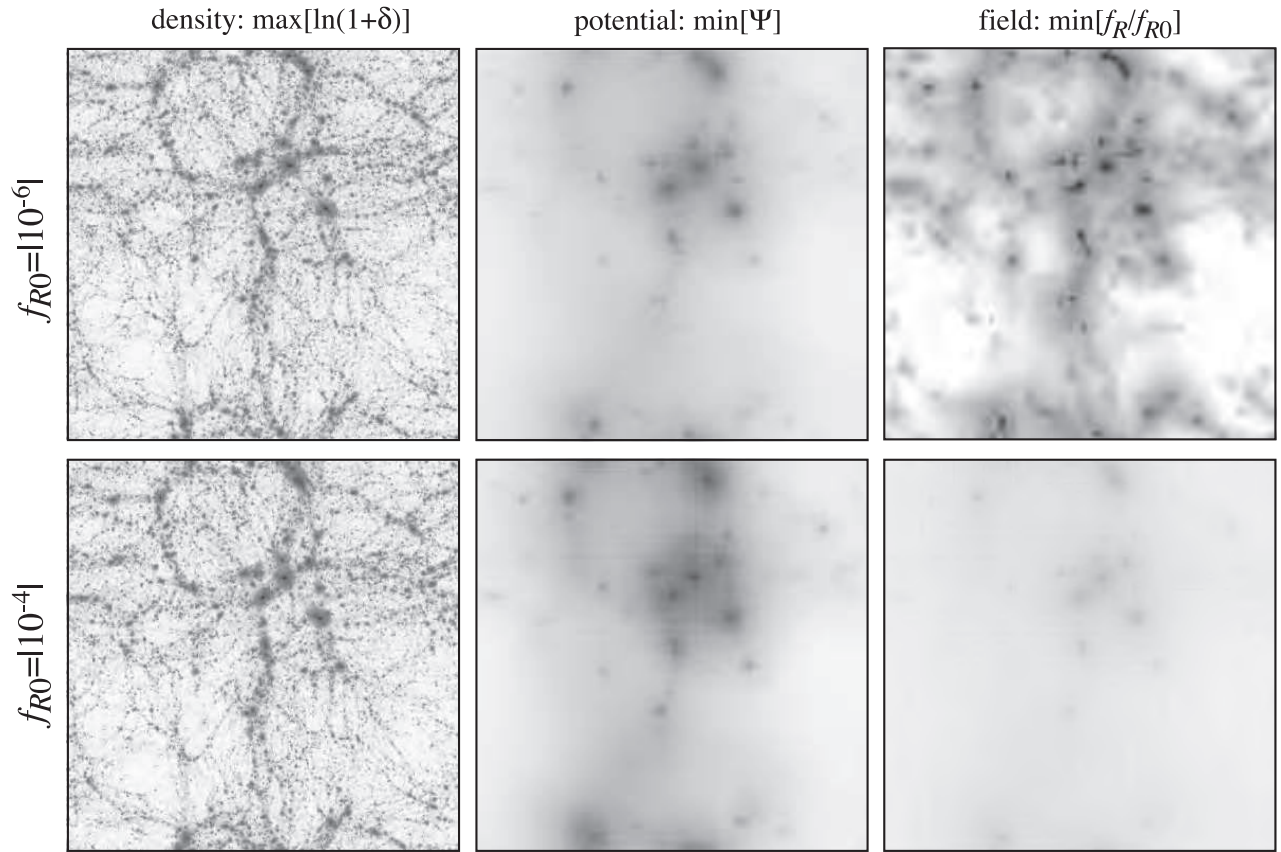


FIG. 3: 2D slices through simulations at  $a = 1$  for various fields: matter overdensity  $\delta \equiv \delta\rho_m/\bar{\rho}_m$  (left); minimum gravitational potential  $\Psi$  along the line of sight (middle) and minimum field  $f_R/f_{R0}$  along the line of sight (right). Each slice has the two dimensions of full  $64h^{-1}$  Mpc box and is projected across  $16h^{-1}$  Mpc along the line of sight. Shading scale ranges from white to black between the extreme field values as follows:  $(-5.0 \rightarrow 9.8)$  for  $\ln(1 + \delta)$ ;  $(0.3 \rightarrow -4.3) \times 10^{-5}$  for  $\Psi$ ;  $(1.05 \rightarrow 0)$  for  $f_R/f_{R0}$ . In the  $f_{R0} = |10^{-6}|$  (top) simulation, the chameleon mechanism suppresses the field and hence the force deviations in the deep potential wells surrounding large overdensities. In the  $f_{R0} = |10^{-4}|$  (bottom) simulation, the  $f_R$  remains stiff and a chameleon does not appear at the present. While the density and potential are slightly enhanced in this run due to the force modification, the appearance of the chameleon depends mainly on the background field value  $f_{R0}$ .

function of Eisenstein & Hu [34] and normalization fixed at high  $z$ . Note that the initial spectrum does not include the effects of baryon acoustic oscillations. The simulations are started at  $z = 49$ , and are integrated in time in steps of  $\Delta a = 0.002$ .

In order to extend the dynamic range of the results, we run three simulations with box sizes  $L_{\text{box}} = 256 h^{-1}$  Mpc,  $128 h^{-1}$  Mpc, and  $64 h^{-1}$  Mpc. All simulations are run with 512 grid cells in each direction and with  $N_p = 256^3$  particles. Thus, the formal spatial resolutions of the simulations are  $0.5 h^{-1}$  Mpc,  $0.25 h^{-1}$  Mpc, and  $0.125 h^{-1}$  Mpc for the largest, middle, and smallest boxes, respectively. The corresponding mass resolutions are  $2.76 \times 10^{11} h^{-1} M_\odot$ ,  $3.45 \times 10^{10} h^{-1} M_\odot$ , and  $4.31 \times 10^9 h^{-1} M_\odot$ .

In the subsequent analysis, the particle Nyquist wave number of each simulation will play important roles in determining the range of trustworthy scales. As shown in [24, 35], power spectrum of cosmological simulations start to show systematic  $> 10\%$  deviations from Smith *et al.* [36] and Peacock & Dodds [37] fits at wave numbers

above half the particle Nyquist mode, defined as  $k_N = \pi N_p^{1/3} / (2L_{\text{box}})$ . For our three simulation sizes, the half-Nyquist wave numbers are, in order of decreasing box size,  $0.79h \text{ Mpc}^{-1}$ ,  $1.57h \text{ Mpc}^{-1}$ , and  $3.14h \text{ Mpc}^{-1}$ .

Finally, to assess the impact of the chameleon mechanism on the power spectrum, we also carry out linearized  $f_R$  simulations in which the gravitational potential,  $\Psi$ , is evaluated according to Eq. (25). In the linearized treatment, the Compton wavelength is assumed to be fixed by the background field and thus chameleon effects are not present. Therefore, the difference between the full  $f_R$  simulations and the linearized  $f_R$  simulations are wholly due to the chameleon effects. To avoid confusion with linearization of the density field, we will call these runs the “no-chameleon” simulations.

For each simulation box configuration, we run multiple simulations with different realizations of the initial power spectrum in order to reduce finite sample variance. The actual number of runs for each configurations are primarily constrained by computational resources and are summarized in Table I. To further reduce the sample

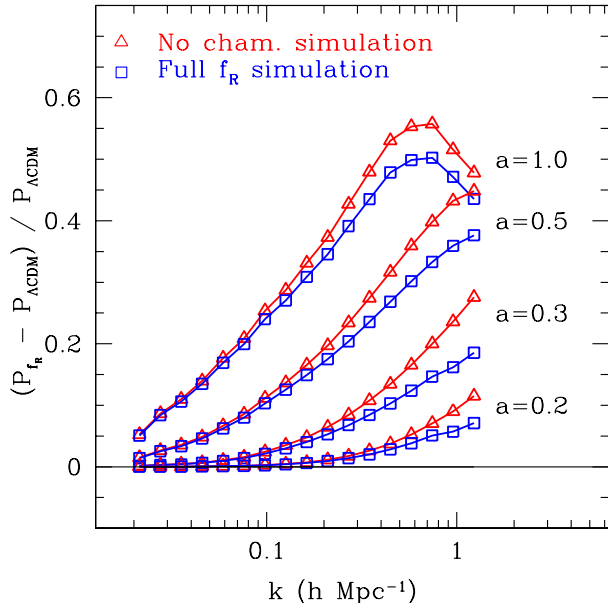


FIG. 4: Evolution of power spectrum deviation for  $f_{R0} = 10^{-4}$  for the full  $f_R$  simulation and the no-chameleon simulation. The appearance of a chameleon at  $a \lesssim 0.5$  causes a large fractional change in the deviations at earlier epochs. As the deviations grow, this offset remains as a smaller fraction of the total.

TABLE I: Simulation type and number

	$ f_{R0} $	$L_{\text{box}} (h^{-1} \text{ Mpc})$		
		256	128	64
# of	$10^{-4}$	5	5	5
boxes	$10^{-5}$	5	5	5
	$10^{-6}$	5	5	5
	0 (GR)	5	5	5
Spatial Resolution ( $h^{-1} \text{ Mpc}$ )		0.5	0.25	0.125
$k_N/2$ ( $h \text{ Mpc}^{-1}$ )		0.79	1.57	3.14
Mass Resolution ( $10^{10} h^{-1} \text{ M}_\odot$ )		27.6	3.45	0.431

variance, we average the difference of the statistics per simulation from the  $\Lambda$ CDM run using the same realizations of the initial conditions.

## B. Power spectrum results

We start with the pure  $\Lambda$ CDM  $f_{R0} = 0$  simulations which serve as the baseline reference for comparison with the other cases. In Fig. 1, we show the average power spectrum in the simulations of the three box sizes. The results from the various box sizes converge below about half the Nyquist wavenumber of the individual boxes. For comparison we also show the fit of Smith *et al.* [36], which scales the linear theory predictions (also shown) into the non-linear regime. The simulations converge to

the accuracy of the fit again at about half the Nyquist wavenumber.

All power spectra shown in this work, unless otherwise specified, are volume-weighted bootstrap-averaged from the multiple simulations of the same cosmological and  $f(R)$  parameters. In the averaging, the power spectra above the respective half-Nyquist modes are disregarded. Similarly, the error bars represent the volume weighted bootstrap error, in which the individual power spectrum data points are assumed to be uncorrelated. We use 2000 bootstrap samples to compute the mean and the error. When we show differences of power spectra, the differencing is performed before averaging.

In the bottom panel of Fig. 1, we show the relative difference between our simulations and the Smith *et al.* power spectra. As expected, the mean simulation power spectrum matches the Smith *et al.* results to  $\sim 10\%$  for all scales of interest. The error bars at the low  $k$  end of the simulation spectrum are large due to the small number of largest scale modes in  $L_{\text{box}} = 256h^{-1} \text{ Mpc}$  box. In the opposite end, the errors are larger due to large variation between the different realizations of  $L_{\text{box}} = 64h^{-1} \text{ Mpc}$  boxes. Note that bootstrap errors are only a rough estimate of the true uncertainties in these regions where the sample size is small.

Fig. 2 shows the power spectrum enhancement of the  $|f_{R0}| = 10^{-6}$  and  $|f_{R0}| = 10^{-4}$  runs relative to the  $\Lambda$ CDM runs. Note that the enhancement of the power spectrum of the lensing potential  $\Phi - \Psi$  is identical by virtue of Eq. (18). For comparison we also plot the linear theory predictions on the relative enhancement [19, 38] and the no-chameleon  $f_R$  simulation. In both the linear theory and the no-chameleon results, the force modification is completely determined by the background field. Thus on all scales smaller than the Compton wavelength in the background there is a sharp enhancement of power. Linear theory tends to overestimate the enhancement due to its neglect of mode coupling which makes the power at high  $k$  dependent on scales out to the non-linear scale where the effects are weaker.

Since non-linear structures can only make the Compton wavelength smaller, the no-chameleon and linear predictions show the maximum scale out to which there are deviations from  $\Lambda$ CDM. However in the full  $f_R$  simulation the chameleon can dramatically change the results at high  $k$  if the background field amplitude is small enough to be overcome by the gravitational potentials of collapsed objects as discussed in §II.

For the  $|f_{R0}| = 10^{-6}$  case the enhancement is reduced by a factor of 4 over the no-chameleon simulations at  $k \approx 1h \text{ Mpc}^{-1}$ . Previous simulations of modified force laws have all been in models where there is no chameleon and no way to hide deviations from ordinary gravity from local measurements [20, 21, 22, 23, 24]. Note that even these reduced  $\sim 1 - 10\%$  enhancements of power are potentially observable in next generation weak lensing surveys (*e.g.* [39, 40]). As expected from the discussion in §II, for the  $|f_{R0}| = 10^{-4}$  model typical gravitational po-

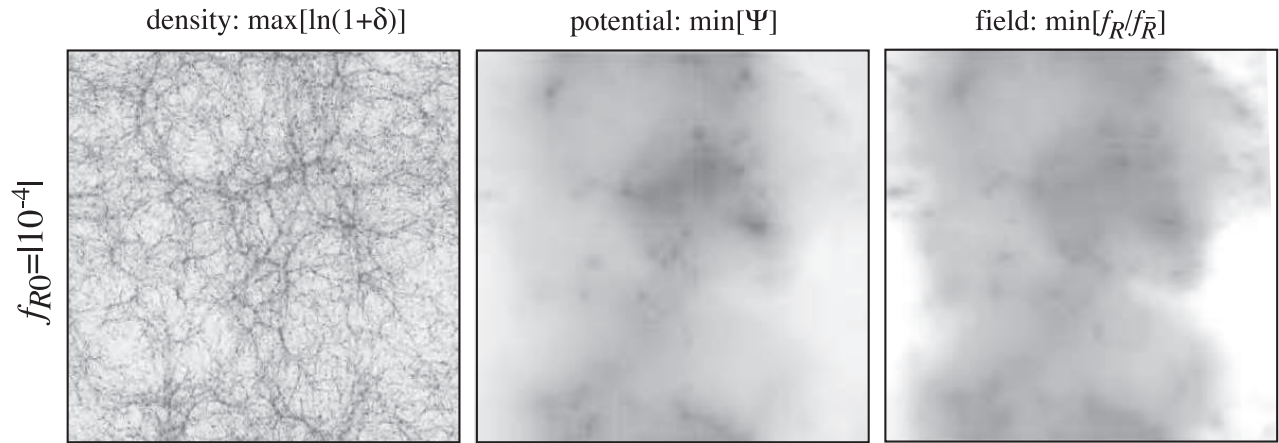


FIG. 5: Same as in Fig. 3 but at  $a = 0.3$  for  $|f_{R0}| = 10^{-4}$  with the field values shown as a fraction of the background field at that time  $\bar{f}_R(a = 0.3)$ . The field amplitude is suppressed in deep potential wells exhibiting a chameleon that suppresses the early growth of structure. The shading scale range for the various fields in this case is also identical to that of Fig. 3.

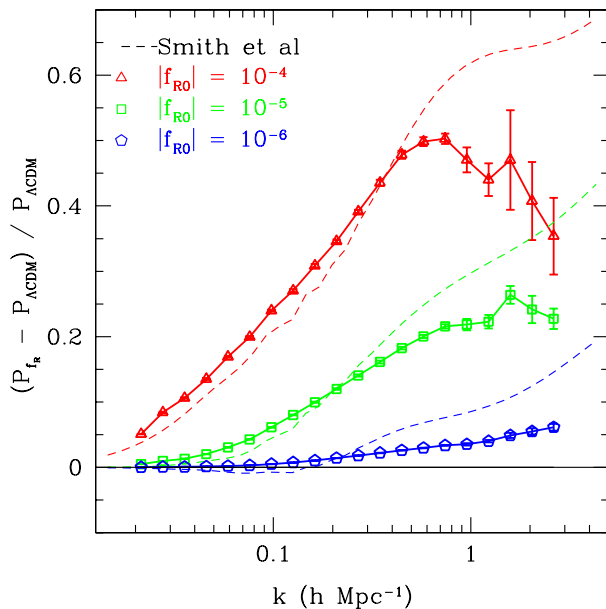


FIG. 6: Power spectrum deviations from  $\Lambda$ CDM of the full  $f_R$  simulations vs. the scaling predictions of Smith *et al.* employing linear  $f_R$  calculations. Note that in all cases the scaling predictions fail to capture the deviations at high  $k$  due both to the change in the abundance and profiles of collapsed objects in the  $f_R$  simulations and the chameleon mechanism.

tentials of order  $10^{-6} - 10^{-5}$  cannot overcome the background field and the chameleon impact is greatly reduced.

By taking slices through the simulations we can see the effects of the environment dependence of the chameleon (see Fig. 3). In the  $|f_{R0}| = 10^{-6}$  run, the  $f_R$  field is suppressed in the high density regions which correspond to deep potential wells. Notice that in low density regions the force law is still modified and this accounts for the small enhancement of power over the  $\Lambda$ CDM case that persists to high  $k$  in Fig. 2. Thus two identical

sets of objects separated by the same distance will feel different forces depending on whether they are located in an overdense or underdense region. Generic tests of gravity such as the comparison between dynamical and lensing mass are predicted to produce null results in sufficiently overdense regions despite the  $\sim 1 - 10\%$  enhancement of power shown in Fig. 2. Conversely, even with a chameleon, substantial modifications to the gravitational force law can appear in voids.

In the  $|f_{R0}| = 10^{-4}$  run, the field remains stiff and at its background value across the whole volume leading to changes in the force law everywhere today. Even in this run, the power spectrum is still suppressed compared with the no-chameleon case (see Fig. 2). This suppression comes about because the background field value was substantially smaller at high redshift. Structures that form during these epochs are again affected by the chameleon and leave an impact at  $z = 0$  as hierarchical structure formation progresses. This can be seen in the evolution of the power spectrum deviations in Fig. 4. The impact of the chameleon at high  $z$  is fractionally large where the overall deviation is small. The offset remains roughly constant at more recent epochs as the overall deviation increases. In Fig. 5 we show slices through the simulation at  $a = 0.3$  that reveal the presence of the chameleon in deep potential wells at that time (*cf.* Fig. 3). The suppression of power spectrum enhancement at  $k \gtrsim 0.7 h \text{ Mpc}^{-1}$  results from the shift of 1-halo contribution to larger scales and the relative flattening of  $\Delta^2(k)$ , as shown in the halo model inspired treatment in [9].

Finally, we can assess how well the Smith *et al.* [36] scaling works in the full  $f_R$  simulations. In Fig. 6 we show that this prescription fails to capture the deviation from  $\Lambda$ CDM at high  $k$ . This disagreement appears for all of the  $f_{R0}$  values and arises both from changes in the contribution of collapsed objects to the power spectrum and the presence of the chameleon effect.

In fact, the whole concept of the linear power spectrum determining the non-linear power spectrum at the same epoch that is shared by Smith *et al.*, the halo model, and other linear to non-linear scaling relations, is flawed in the context of a modification to gravity that evolves with redshift. We have seen that the precise form of the  $z = 0$  power spectrum in the  $|f_{R0}| = 10^{-4}$  runs depends on the presence or absence of a chameleon at a higher redshift. This information is not directly encoded in the linear power spectrum.

#### IV. DISCUSSION

We have carried out the first cosmological simulations of  $f(R)$  models for cosmic acceleration that exhibit the chameleon mechanism. The chameleon mechanism involves a non-linear field equation for the scalar degree of freedom that suppresses the range of the gravitational force modification or Compton scale in the deep gravitational potential wells of cosmological and astrophysical structure. We have here focused on its impact on the matter power spectrum or equivalently the potential power spectrum relevant for weak lensing surveys. While we have simulated only one particular functional form of  $f(R)$ , we expect that the qualitative behavior of other models that exhibit a chameleon behavior to yield similar results once scaled to the appropriate Compton scales and field amplitudes.

In the absence of the chameleon mechanism, gravitational interactions would have an enhancement of a factor of 4/3 on all scales smaller than the Compton scale in the cosmological background eventually leading to order unity enhancements in the power at high wavenumber. The chameleon mechanism turns on when the depth of the local gravitational potential becomes comparable to the field amplitude in the background. We have shown through otherwise identical simulations of structure with the chameleon mechanism artificially turned off that once the chameleon appears, it causes a substantial reduction of the enhanced power. For example, for a field amplitude of  $|f_{R0}| = 10^{-6}$  the change in the enhancement of power at  $k \sim 1h^{-1}\text{Mpc}$  is a factor of four.

Even in cases where current cosmological structures do not possess a chameleon ( $|f_{R0}| \gtrsim 10^{-5}$ ), there still is an impact on the power spectrum due to evolutionary effects. In  $f(R)$  models where the field amplitude decreases with curvature, the chameleon can appear again at high redshift when the building blocks of current structure were assembled.

Scaling relations which take the linear power spectrum and map it into the non-linear regime qualitatively misestimate the non-linear power spectrum in several ways. For example, the Smith *et al.* [36] prescription assumes that the non-linear power spectrum depends only on the shape of the linear power spectrum near the non-linear scale. This prescription fails to describe both the chameleon mechanism and the change in the structure and abundance of collapsed objects leading to a severe misestimate at high  $k$ .

A halo model can in principle do better to model these effects but simple prescriptions that scale the mass function to the linear variance and leave halo profiles unchanged also do not describe the non-linear effects to sufficient accuracy (*cf.* [9]). In the next paper of this series, we intend to study the impact of  $f(R)$  modifications on halo properties.

*Acknowledgments:* We thank N. Dalal, B. Jain, J. Khoury, K. Koyama, A. Kravtsov, A. Upadhye, I. Sawicki, F. Schmidt, J. Tinker, and F. Stabenau for useful conversations. This work was supported in part by the Kavli Institute for Cosmological Physics (KICP) at the University of Chicago through grants NSF PHY-0114422 and NSF PHY-0551142 and an endowment from the Kavli Foundation and its founder Fred Kavli. HO was additionally supported by the NSF grants AST-0239759, AST-0507666, and AST-0708154 at the University of Chicago. WH and ML were additionally supported by U.S. Dept. of Energy contract DE-FG02-90ER-40560 and WH by the David and Lucile Packard Foundation. Some of the computations used in this work have been performed on the Joint Fermilab - KICP Supercomputing Cluster, supported by grants from Fermilab, Kavli Institute for Cosmological Physics, and the University of Chicago.

- 
- [1] A. I. Vainshtein, Phys. Lett. **B39**, 393 (1972).
  - [2] C. Deffayet, G. R. Dvali, G. Gabadadze, and A. I. Vainshtein, Phys. Rev. **D65**, 044026 (2002), hep-th/0106001.
  - [3] G. Dvali, New J. Phys. **8**, 326 (2006), hep-th/0610013.
  - [4] A. D. Dolgov and M. Kawasaki, Phys. Lett. **B573**, 1 (2003), astro-ph/0307285.
  - [5] I. Sawicki and W. Hu, Phys. Rev. **D75**, 127502 (2007), astro-ph/0702278.
  - [6] M. D. Seifert, Phys. Rev. **D76**, 064002 (2007), gr-qc/0703060.
  - [7] A. Lue, R. Scoccimarro, and G. D. Starkman, Phys. Rev. **D69**, 124015 (2004), astro-ph/0401515.
  - [8] K. Koyama and F. P. Silva, Phys. Rev. **D75**, 084040 (2007), hep-th/0702169.
  - [9] W. Hu and I. Sawicki, Phys. Rev. D **76**, 104043 (2007), arXiv:0708.1190.
  - [10] T. P. Sotiriou and V. Faraoni (2008), 0805.1726.
  - [11] S. M. Carroll, V. Duvvuri, M. Trodden, and M. S. Turner, Phys. Rev. **D70**, 043528 (2004), astro-ph/0306438.
  - [12] S. Nojiri and S. D. Odintsov, Phys. Rev. **D68**, 123512 (2003), hep-th/0307288.
  - [13] S. Capozziello, S. Carloni, and A. Troisi, Recent Res. Dev. Astron. Astrophys. **1**, 625 (2003), astro-ph/0303041.



- [14] T. Chiba, Phys. Lett. **B575**, 1 (2003), astro-ph/0307338.
- [15] T. Chiba, T. L. Smith, and A. L. Erickcek (2006), astro-ph/0611867.
- [16] J. Khoury and A. Weltman, Phys. Rev. D **69**, 044026 (2004), arXiv:astro-ph/0309411.
- [17] I. Navarro and K. Van Acoleyen, JCAP **0702**, 022 (2007), gr-qc/0611127.
- [18] T. Faulkner, M. Tegmark, E. F. Bunn, and Y. Mao, Phys. Rev. **D76**, 063505 (2007), astro-ph/0612569.
- [19] W. Hu and I. Sawicki, Phys. Rev. D **76**, 064004 (2007), arXiv:0705.1158.
- [20] M. J. White and C. S. Kochanek, Astrophys. J. **560**, 539 (2001), astro-ph/0105227.
- [21] A. V. Maccio, C. Quercellini, R. Mainini, L. Amendola, and S. A. Bonometto, Phys. Rev. **D69**, 123516 (2004), astro-ph/0309671.
- [22] A. Nusser, S. S. Gubser, and P. J. E. Peebles, Phys. Rev. **D71**, 083505 (2005), astro-ph/0412586.
- [23] H. F. Stabenau and B. Jain, Phys. Rev. **D74**, 084007 (2006), astro-ph/0604038.
- [24] I. Laszlo and R. Bean, Phys. Rev. **D77**, 024048 (2008), 0709.0307.
- [25] H. Oyaizu, ArXiv e-prints (2008), astro-ph/0807.2449.
- [26] D. N. Spergel, R. Bean, O. Doré, M. R. Nolta, C. L. Bennett, J. Dunkley, G. Hinshaw, N. Jarosik, E. Komatsu, L. Page, et al., Astrophysical Journal, Supplement **170**, 377 (2007), arXiv:astro-ph/0603449.
- [27] P. Zhang, Phys. Rev. **D73**, 123504 (2006), astro-ph/0511218.
- [28] G. R. Dvali, G. Gabadadze, and M. Porrati, Phys. Lett. **B485**, 208 (2000), hep-th/0005016.
- [29] C. M. Will, Living Reviews in Relativity **9** (2006), URL <http://www.livingreviews.org/lrr-2006-3>.
- [30] A. Brandt, Proceedings of Third International Conference on Numerical Methods in Fluid Mechanics (1973).
- [31] W. L. Briggs, V. E. Henson, and S. F. McCormick, *A multigrid tutorial (2nd ed.)* (Society for Industrial and Applied Mathematics, Philadelphia, PA, USA, 2000), ISBN 0-89871-462-1.
- [32] Y.-S. Song, H. Peiris, and W. Hu, Phys. Rev. D **76**, 063517 (2007), arXiv:0706.2399.
- [33] B. W. O'Shea, G. Bryan, J. Bordner, M. L. Norman, T. Abel, R. Harkness, and A. Kritsuk, ArXiv Astrophysics e-prints (2004), astro-ph/0403044.
- [34] D. J. Eisenstein and W. Hu, Astrophys. J. **496**, 605 (1998), arXiv:astro-ph/9709112.
- [35] H. F. Stabenau and B. Jain, Phys. Rev. D **74**, 084007 (2006), arXiv:astro-ph/0604038.
- [36] R. E. Smith, J. A. Peacock, A. Jenkins, S. D. M. White, C. S. Frenk, F. R. Pearce, P. A. Thomas, G. Efstathiou, and H. M. P. Couchman, Mon. Not. R. Astron. Soc. **341**, 1311 (2003), arXiv:astro-ph/0207664.
- [37] J. A. Peacock and S. J. Dodds, Mon. Not. R. Astron. Soc. **280**, L19 (1996), arXiv:astro-ph/9603031.
- [38] L. Pogosian and A. Silvestri, Phys. Rev. D **77**, 023503 (2008), arXiv:0709.0296.
- [39] W. Hu, Phys. Rev. **D66**, 083515 (2002), astro-ph/0208093.
- [40] L. Knox, Y.-S. Song, and J. A. Tyson, Phys. Rev. **D74**, 023512 (2006).